Thiabendazole Inhibits Glioblastoma Cell Proliferation and Invasion Targeting Mini-chromosome Maintenance Protein 2[S]

Yaotian Hu, Wenjing Zhou, Zhiyi Xue, Xuemeng Liu, Zichao Feng, Yulin Zhang, Xiaofei Liu, Wenjie Li, Qing Zhang, Anjing Chen, Bin Huang, and Jian Wang

Department of Neurosurgery (Y.H., W.Z., Z.X., X.L., Z.F., Y.Z., X.L, W.L., Q.Z., A.C., B.H., J.H.), Qilu Hospital and Institute of Brain and Brain-Inspired Science, Cheeloo College of Medicine, Shandong University, Jinan, China; Shandong Key Laboratory of Brain Function Remodeling, Jinan, China; and Department of Biomedicine (J.W.), University of Bergen, Jonas Lies vei 91, 5009 Bergen, Norway

ABSTRACT

Thiabendazole (TBZ), approved by the US Food and Drug Administration (FDA) for human oral use, elicits a potential anticancer activity on cancer cells in vitro and in animal models. Here, we evaluated the efficacy of TBZ in the treatment of human glioblastoma multiforme (GBM). TBZ reduced the viability of GBM cells (P3, U251, LN229, A172, and U118MG) relative to controls in a dose- and time-dependent manner. However, normal human astrocytes (NHA) exhibited a greater IC_{50} than tumor cell lines and were thus more resistant to its cytotoxic effects. 5-Ethynyl-2′-deoxyuridine (EdU)-positive cells and the number of colonies formed were decreased in TBZ-treated cells (at 150 μM, $P < 0.05$ and at 150 μM, $P < 0.001$, respectively). This decrease in proliferation was associated with a G2/M arrest as assessed with flow cytometry, and the downregulation of G2/M check point proteins. In addition, TBZ suppressed GBM cell invasion. Analysis of RNA sequencing data comparing TBZ-treated cells with controls yielded a group of differentially expressed genes, the functions of which were associated with the cell cycle and DNA replication. The most significantly downregulated gene in TBZ-treated cells was mini-chromosome maintenance protein 2 (MCM2). SiRNA knockdown of MCM2 inhibited proliferation, causing a G2/M arrest in GBM cell lines and suppressed invasion. Taken together, our results demonstrated that TBZ inhibited proliferation and invasion in GBM cells through targeting of MCM2.

SIGNIFICANCE STATEMENT

TBZ inhibits the proliferation and invasion of glioblastoma cells by downregulating the expression of MCM2. These results support the repurposing of TBZ as a possible therapeutic drug in the treatment of GBM.

Introduction

Glioblastoma multiforme (GBM) is the most common and malignant primary brain tumor in human adults, with only 14.6 months of median survival after primary diagnosis (Darlix et al., 2017), despite a standard therapeutic regimen consisting of surgery, radiotherapy, and chemotherapy (Ostrom et al., 2020). The current chemotherapy used is often temozolomide, an oral DNA alkylating agent, which in combination with radiotherapy following surgery has increased patient survival from 12.1 to 14.6 months (Stupp et al., 2005). However, at least 50% of patients with GBM do not respond (Lee, 2016). Several biologic properties of GBM render the disease resistant to treatment. First, GBM cells filtrate the peripheral normal brain tissue, making complete removal of the tumor with surgery impossible (Bell and Karnosh, 1949; Shergalis et al., 2018). Second, most chemotherapeutic molecules insufficiently permeate the brain due to the blood-brain barrier (Shergalis et al., 2018). Third, targeting of key molecular pathways is ineffective because of the high cellular and genetic heterogeneity within GBM (Brennan et al., 2013). Thus, novel effective drugs and therapeutic targets are urgently needed for GBM treatment.

Drug repurposing has become a widely accepted strategy in oncology to identify new therapies. Drugs already known to be safe in humans accelerate the initiation of needed clinical trials, especially in the case of cancers with few treatment options. For instance, flubendazole and mebendazole are benzimidazole carbamate family compounds approved for use as anthelminthics in humans and have been studied for their anticancer properties against diverse cancers, including human glioma.

ABBREVIATIONS: CCK-8, Cell Counting Kit-8; CDK1, cyclin dependent kinase 1; DAP I, 4′,6-diamidino-2-phenylindole; EdU, 5-Ethynyl-2′-deoxyuridine; GBM, glioblastoma multiforme; GAPDH, glyceraldehyde-3-phosphate dehydrogenase; MCM2, mini-chromosome maintenance protein 2; MMP2, matrix metalloproteinase 2; NHA, normal human astrocytes; PCNA, proliferating cell nuclear antigen; TBZ, thiabendazole; ZEB1, zinc finger E-box binding homeobox 1.

Flubendazole has been shown to inhibit glioma proliferation and tumorigenesis. Mebendazole was shown to be cytotoxic to glioma and significantly prolonged mean survival in syngeneic and xenograft orthotopic animal glioma models (Bai et al., 2011). In a phase 1 clinical trial, mebendazole demonstrated long-term safety and acceptable toxicity at doses of up to 200 mg/kg (Gallia et al., 2021). Another benzimidazole, thiabendazole [TBZ; tiabendazole; 2-(thiazol-4-yl) benzimidazole], has been used to treat gut parasites in humans for over 50 years (Campbell and Cuckler, 1969; Whalen et al., 1971). TBZ inhibits blastocysts, candida albicans, penicillium, and psoriasis and prevents the formation of aflatoxin in plant feed, but it does not affect carcinogenesis and fertility in animals (Gosselin et al., 1984). A previous study demonstrated that TBZ reduced the growth of human fibrosarcoma (Cha et al., 2012). Therefore, as a non-toxic member of the family of benzimidazole compounds, TBZ has gained interest for its potential as an anticancer therapy in humans.

In this study, we examined the anticancer effects of TBZ and investigated its potential molecular mechanisms in GBM cells in vitro and in vivo. We demonstrated that TBZ induces G2/M arrest in GBM cells and inhibits invasion. We performed RNA sequencing on the tumor cells treated with TBZ to identify differentially expressed genes and found mini-chromosome maintenance protein 2 (MCM2) to be a key transcriptional factor downregulated by TBZ, showing the MCM2 as a molecular target of TBZ. Finally, we determined that TBZ inhibits GBM cell growth in vivo.

Materials and Methods

Ethics Statement. Nude mice (age, 4 weeks; weight, 14 to 17 g) were purchased from the Nanjing Biomedical Research Institute of Nanjing University (Nanjing, China) and maintained in the animal facility of Qilu Hospital, Shandong University under pathogen-free conditions. Ethical approval was granted by the Ethics Committee/ Laboratory Animal Research Center protocols of Qilu Hospital, Shandong University (Jinan, China).

Cell Lines and Cultures. GBM cell lines, U251, LN229, A172, U118MG, and normal human astrocytes (NHA) were purchased from by the Chinese Academy of Sciences Cell Bank (Shanghai, China) and authenticated by short tandem repeat (STR) profiling. The cells are anchorage-dependent cells in the absence of any stress. Complete medium for NHA, U251, LN229, A172, and U118MG is made up of the following reagents: Dulbecco's modified Eagle's medium (DMEM; Thermo Fisher Scientific; Waltham, MA, USA), 10% fetal bovine serum (FBS; Thermo Fisher Scientific), streptomycin (100 U/ml) and penicillin (100 U/ml). The cells were cultured in a humidified incubator (HERAcell 204i, ThermoFisher Scientific) at 37°C, 5% CO_2.

The P3 cells used in the study were derived from primary human GBM cells and were cultured in Neurobasal Medium (NBM; 21103-049, ThermoFisher Scientific) supplemented with 2% B27 (cat#-A3653401, ThermoFisher Scientific), 1% L-glutamine (BE17-605E, BioNordika; Oslo, Norway), 1% penicillin/streptomycin (17-603E, BioNordika), 20 ng/ml of EGF (AF-100-15, Peprotech; Rocky Hill, NJ, USA), and 20 ng/ml bFGF (100-18B, Peprotech) in a humidified incubator at 37°C, 5% CO_2. The cells were sub-cultured every 3 days at a sub-culture ratio of 1:3. A PCR-based assay was used to detect mycoplasma contamination.

Antibodies and Reagents. Mini-chromosome maintenance complex component 2 (MCM2, western-blotting dilution 1:1000), cyclin dependent kinase 1 (CDK1, western-blotting dilution 1:1000), cyclin B1 (western-blotting dilution 1:1000), N-cadherin (western-blotting dilution 1:1000), zinc finger E-box binding homeobox 1 (ZEB1, western-blotting dilution 1:1000) and glyceraldehyde-3-phosphate dehydrogenase (GAPDH, western-blotting dilution 1:1000) were purchased from Cell Signaling Technology (Danvers, MA, USA).

Actin beta (ACTB, β-actin, western-blotting dilution 1:1000), proliferating cell nuclear antigen (PCNA, western-blotting dilution 1:1000), cyclin B2 (western-blotting dilution 1:1000) and Ki67 (Immunohistochemistry dilution 1:200) were purchased from Abcam (Cambridge, UK).

Mini-chromosome maintenance complex component 5 (western-blotting dilution 1:1000), matrix metalloproteinase 2 (MMP2, western-blotting dilution 1:1000) were purchased from Proteintech (Rosemont, IL, USA).

Ubiquitin with PHD and ring finger domains 1 (western-blotting dilution 1:1000) were purchased from Santa Cruz (Dallas, TX, USA).

Horseradish peroxidase-labeled goat anti-rabbit secondary antibodies were provided by Zhongshan Golden Bridge Bio-technology (Beijing, China). Proteins on western blots were measured with enhanced chemiluminescence (Millipore; Burlington, MA, USA). The PI/RNase staining buffer kit was provided from BD Pharmingen (San Diego, CA, USA).

TBZ (45684, Sigma-Aldrich; St. Louis, MO, USA) was dissolved in dimethyl sulfoxide (DMSO; D2650, Sigma-Aldrich) at a concentration of 100 mM, stored at -20°C, and diluted to working concentrations in culture medium when needed. The diluted TBZ was used within 1 month.

The 96-well 3D spheroid cell reagent kit (3500-096-K, Cultrex) was purchased from Trevigen (Gaithersburg, MD, USA).

Cell Viability Assay. Cell Counting Kit-8 assay (CCK-8; Dojindo, Kumamoto, Japan) was used to assess cell viability. GBM cells (4×10^3) were seeded into each well of 96-well plates (Corning; Corning, NY, USA) and cultured in a humidified incubator at 37°C, 5% CO_2. After 24 hours, the medium was replaced with 100 μl of fresh culture medium containing different concentrations of TBZ or vehicle control (DMSO). At 24, 48, 72, and 96 hours after dosing, GBM cells were incubated with 10 μl of CCK-8 reagent in 100 μl of serum-free DMEM at 37°C for 1 hour and an EnSight Multimode Plate Reader (PerkinElmer; Singapore) was used to measure the absorbance at 450 nm. Cell viability of GBM cells transfected with MCM2 siRNA and overexpression constructs was also assessed with the CCK-8 assay.

Cell Proliferation Assay. GBM cells (1×10^4) were seeded into each well of 24-well plates (Corning) and cultured in a humidified incubator at 37°C, 5% CO_2. 5-ethynyl-2'-deoxyuridine (EdU) was diluted 1:1000 in DMEM complete medium, and GBM cells were treated with the EdU mixed medium for 1 hour. EdU was detected through a catalyzed reaction between EdU and Apollo fluorescent dyes provided in the EdU incorporation assay (C103103, Ribobio; Guangzhou, China). Apollo dying solution was prepared as follows: 4690 μl of distilled water, 250 μl of Apollo reaction buffer, 50 μl of Apollo catalyst solution, 15 μl of Apollo fluorescent dye solution, and 44 mg of Apollo buffer additive. Two hundred fifty microliters of Apollo dying solution was added to each well. Nuclei were counterstained with 4',6-diamidino-2-phenylindole (DAPI), and EdU-positive cells were counted under fluorescence microscopy (Leica; Solms, Germany).

Colony Formation Assay. U251 and P3 cells were counted, the cell density was diluted to 500 cells/ml, and 2 ml of the cell suspension was added to each well of a 6-well plate (Corning). The drug concentrations used were as follows: 0 μM (DMSO), 150 μM, and 300 μM, following 7 days of culturing. The medium was then replaced with fresh medium, and cells were continued culture for an additional 7 days. The culture medium was discarded, each well of the 6-well plate was rinsed with 500 μl of PBS (3×), and the cells were fixed with 4% paraformaldehyde for 15 minutes. Each well of the 6-well plate was rinsed with 500 μl of PBS (3×), and cells were stained for 30 minutes with crystal violet. The wells were slowly rinsed with double distilled water. After air drying the wells, clones were counted if the number of cells was >50.

Protein Lysates and Western Blotting. GBM cells were lysed with RIPA Lysis Buffer (Beyotime; Shanghai, China) supplemented with phenylmethanesulfonyl fluoride (PMSF, Beyotime) for 30 minutes after 48 hours of treatment. Lysates were centrifuged at 13,000 rpm/min for 20 minutes (Centrifuge 5804R, Thermo Fisher Scientific), and protein concentrations were assessed with the BCA assay according to the manufacturer's instructions (Beyotime, China).

The PAGE Gel Fast Preparation Kit (PG112, Epizyme, Shanghai, China, 4°C storage) was used to prepare 1.5-mm-thick, 10% gels with 15 wells according to the manufacturer's instructions.

Cell lysates (20 μg protein) were subjected to western blot analysis, according to previously described protocols (Kong et al., 2019). Membranes were incubated with primary antibody at 4°C overnight followed by incubation with appropriate secondary antibodies (1:2000) for 1 hour at room temperature. Chemiluminescent signals were imaged using the Chemiluminescence Imager (Bio-Rad; Hercules, CA, USA) according to the manufacturer's protocol. Band density was quantified with ImageJ software and normalized to GAPDH or β-actin. All experiments were repeated three times.

Cell Cycle. U251 and P3 cells were diluted to 4×10^5 cells/ml, and 2 ml of the cell suspension was seeded into each well of a 6-well plate and cultured overnight. TBZ was added to cells at the following concentrations: 0 μM (DMSO), 150 μM, and 300 μM. After 2 days, cells were rinsed and harvested at 4000 rpm/min for 5 minutes, and gently fixed in 300 μl of fresh PBS and 700 μl of 75% ethanol. Cells were incubated at 4°C overnight, harvested at 4000 rpm/min for 5 minutes, and rinsed with PBS at 4000 rpm/min for 5 minutes. The cell pellets were stained with propidium iodide (PI, BD Biosciences; San Jose, CA, USA) dye solution for 20 minutes and then followed by flow cytometry for cell cycle analysis. In gate P1, the linear relationship was set for F2L-A and F2L-H. Gate P2 is looped to select diploid and tetraploid cells, and 10,000 events were collected under P2 conditions. Data were exported, and Modifit 2.0 software was used to determine the cell cycle distribution. GBM cells transfected with MCM2 siRNA and MCM2 overexpression constructs were similarly processed to obtain cell cycle parameters.

Trans-well Invasion Assay. U251 and P3 cells were diluted to 4×10^5 cells/ml, and 2 ml of cell suspension was seeded into each well of a 6-well plate. The cells were incubated under different conditions for 48 hours. Transwell migration plates with an 8-μm pore size (Corning; Sigma-Aldrich) were coated with Matrigel (Becton-Dickinson; Bedford, MA, USA) for 4 hours. The upper chamber of a transwell apparatus was seeded with 20,000 cells in 100 μl of DMEM without FBS and 600 μl of medium containing 10% FBS was added to the lower chamber. After 24-hour incubation at 37°C, the remaining cells were removed from the top side of the insert with a cotton swab, and the migrated cells were fixed with 4% paraformaldehyde for 15 minutes, rinsed twice with PBS, and stained with crystal violet for 30 minutes. The dye was removed, and cells were rinsed with double distilled water. Images from three random views under a light microscope were acquired and used to count migrated cells.

Cell Invasion in 3D Culture. Three thousand cells were seeded into each well of the 3D Culture Qualified 96-well spheroid formation plates (Trevigen) with 100 μl of medium and cultured at 37°C, 5% CO_2 for 72 hours in a humidified incubator. After 72 hours, U251 and P3 cells formed tumor spheroids. Plates were placed on ice for 15 minutes, and 50 μl of invasion matrix (Trevigen, 3500-096-03) was added to each well in the plates. Plates were centrifuged at 300×g at 4°C for 5 minute and incubated at 37°C for 1 hour. Conditioned medium (100 μl) with different concentrations of TBZ was added to each well of the plates. P3 tumor spheroids were incubated for 3 days, and U251 tumor spheroids were incubated for 10 days. Images of the spheroids were captured every 24 hours under bright field microscopy with a 4× objective. The 192-hour images of U251 and the 48-hour images of P3 were analyzed with the software ImageJ. GBM cells after transfection with MCM2 siRNA or MCM2 overexpression constructs were also assessed in 3D invasion culture as described above.

RNA-Seq and Bioinformatics Analysis. The RNA-Seq libraries were prepared using the Illumina TruSeq RNA sample preparation kit (Illumina, San Diego, CA) and sequenced through paired-end (150 base paired-end reads) sequencing performed on the Illumina Nova-SEq. 6000 platform. Raw data were then quality filtered to generate "clean reads" for further analysis. The clean reads were aligned to the human genome reference (hg19) using STAR software and the reference-based assembly of transcripts was conducted using HISAT2. We used picard to compare the results and to remove redundancy and used Sentieon software to detect single-nucleotide variations and InDels. All previously identified single-nucleotide variations and InDels were determined using the dbsnp database. Gene expression values were expressed as reads per kilobase of exon per million fragments mapped using kallisto software. To identify true differentially expressed genes, the false discovery rate was used for the rectification of the P values. The differentially expressed genes (P value $\leq$ 0.05, |Log2FC|$\geq$1) were subjected to enrichment analyses of gene ontology and Kyoto Encyclopedia of Genes and Genomes pathways. Protein-to-protein interaction network analyses of differentially expressed genes was performed using the STRING database, and the protein–protein interaction networks were visualized with Cytoscape software.

RNA Interference. GenePharma (Shanghai, China) used BLAST (www.ncbi.nlm.nih.gov/BLAST/) to select an appropriate target sequence and synthesized siRNAs. Interfering RNA sequences (siRNA) targeting human MCM2 (Gene Pharma Gene; Shanghai, China) were transfected into cells with Lipofectamine 2000 reagent (Thermo Fisher Scientific) according to the manufacturer's protocol. Western blot was used to determine the knockdown efficiency 48 hours after transfection. SiRNA sequences used were the following: Negative control (sense 5'-UUC UCC GAA CGU GUC ACG UTT-3', antisense 5'-ACG UGA CAC GUU CGG AGA ATT-3'), MCM2-Homo-799 (sense 5'-GUG GUG AAC UAU GAG GAC UTT-3', antisense 5'-AGU CCU CAU AGU UCA CCA CTT-3'), MCM2-Homo-1211 (sense 5'-CCA UCU AUC AGA ACU ACC ATT-3', antisense 5'-UGG UAG UUC UGA UAG AUG GTT-3'), MCM2-Homo-1355 (sense 5'-GCA UCU AUC ACA ACU AUU-3', antisense 5'-UAG UUG UUG UGA UAG AUG CTT-3').

Lentiviral Transduction. Lentiviral vectors expressing human mRNA targeting MCM2 (GenePharma, Shanghai) or scrambled-control (negative control) were used to generate stable cell clones overexpressing MCM2 or a nonspecific RNA as the control. Transfected clones were selected in 1 mg/ml of puromycin (Selleckchem; Houston, TX, USA) for 2 weeks. Western blot analysis was used to evaluate the transduction efficiency.

Orthotopic Xenograft Model. P3 cells expressing luciferase-GFP (X×10X; OBiO Technology; Shanghai, China) were implanted into the brains of nude mice. After 7 days, tumor was determined using bioluminescence imaging (PerkinElmer IVIS Spectrum; Waltham, MA, USA), and the mice were divided into the following two groups: control, $n = 5$; TBZ, $n = 5$. Mice were intraperitoneally injected with diluted DMSO alone (control) and TBZ (50 mg/kg per day) every day. Tumor volume was monitored using the bioluminescence imaging every week for 3 weeks, and the weight of each mouse was recorded every week for 4 weeks. Tumor-bearing nude mice were treated until severe symptoms or death appeared imminent: the body weight had decreased >10%, and mice were unable to return upright after being pushed down. Survival (in days) was determined as the number of days starting from implantation (day 1) to death. Mice were euthanized at the end of the experiment. Excised tumor tissue was snap frozen in liquid nitrogen or formalin-fixed for further analysis.

Liquid Chromatography–Tandem Mass Spectrometry Analysis. The nude mice were separated into TBZ-treated group (intraperitoneal injection, three mice) and control group (three mice). Two hours after the injection, the mice were anesthetized with chloral hydrate solution (Qilu hospital, China). PBS was perfused through the heart. The mice were sacrificed by CO_2 inhalation and the brain samples were collected and stored at −80°C. The TBZ and the brain samples were further analyzed by liquid chromatography–tandem
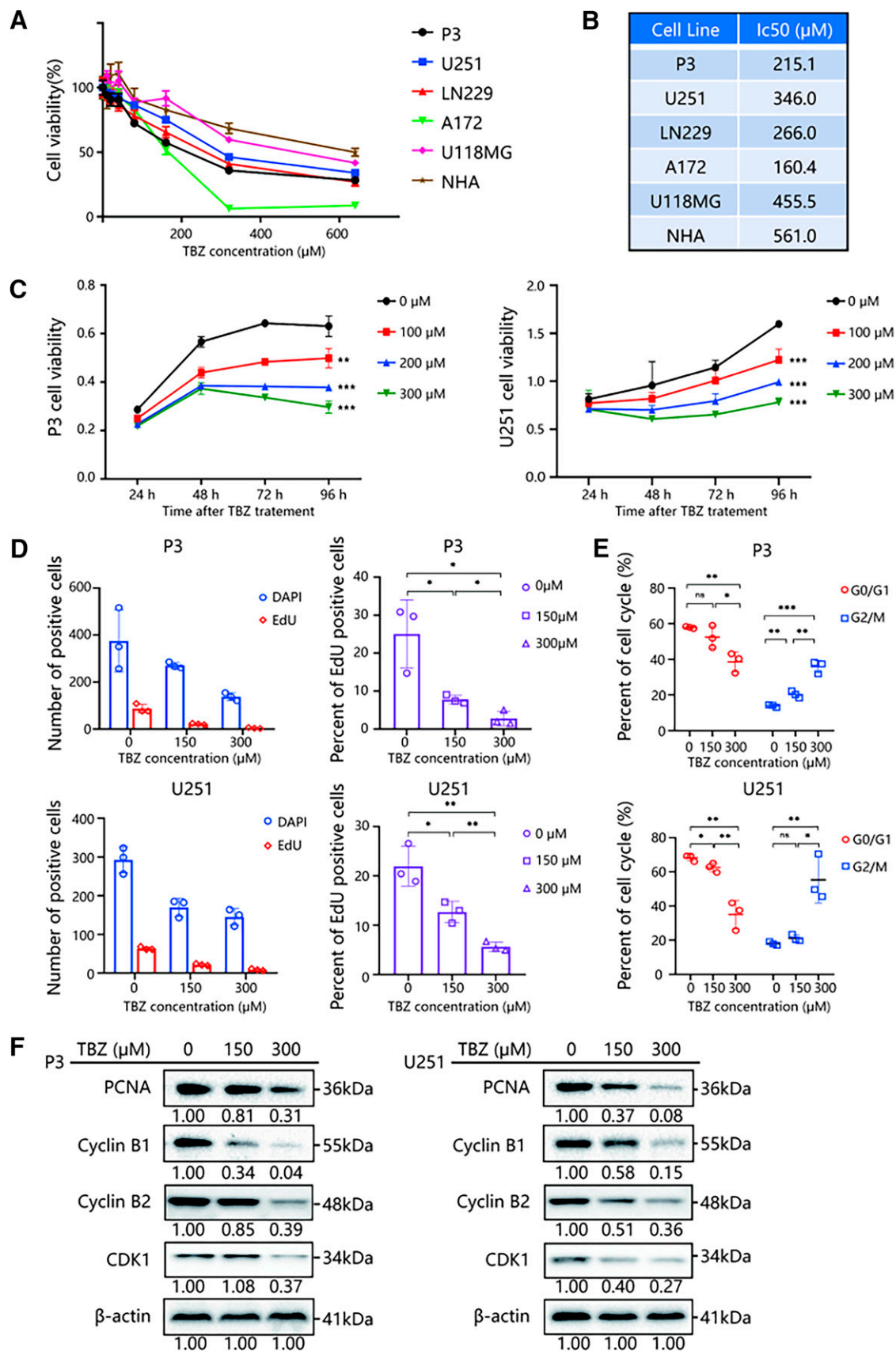
Fig. 1. Thiabendazole (TBZ) promotes G2/M arrest in glioblastoma multiforme cells in vitro. (A) Cell Counting Kit-8 assays to measure cell viability of P3, U251, LN229, A172, U118MG, and NHA treated with TBZ at different concentrations for 48 hours. Data points represent the percentage (%; OD450 treated/OD450 untreated) relative to untreated cells. (B) IC$_{50}$ value of cell lines P3, U251, LN229, A172, U118MG, and NHA calculated with GraphPad Prism 8. (C) Cell Counting Kit-8 assays to measure cell viability of P3 and U251 with TBZ at different concentrations

mass spectrometry to examine the distribution of TBZ within the brain tissue. In brief, the tissue samples were weighed, and appropriate amounts of methanol (chromatographically pure; Thermo Fisher, USA) and zirconia grinding beads were added (Servicebio, Wuhan, China). The samples were ground for 5 minutes after vortexing for 10 minutes and then centrifuged at 15,000 RPM for 10 minutes (centrifuge: D3024R, Dragonlab, Beijing, China). The supernatant was collected and diluted for the analysis on the UltiMate 3000 RS (ThermoFisher Scientific, USA) and TSQ Quantum (ThermoFisher Scientific, USA) instruments.

Plotting and Statistical Analysis. Each assay was independently conducted at least three times. All analyses were performed using GraphPad Prism 8.02 software (San Diego, CA, USA). Data were reported as the mean ± S.D. The statistical significance of data were evaluated using a Student's t-test, and the following P values were considered significantly different: $*P < 0.05$; $**P < 0.01$; $***P < 0.001$.

Results

Thiabendazole Induces G2/M Arrest in GBM Cells. To determine whether TBZ is cytotoxic to GBM, we first exposed GBM cell lines and NHA to TBZ in vitro. The viability of all cells tested, including P3, U251, LN229, A172, U118MG, and NHA, decreased in a dose-dependent manner with increasing concentrations of TBZ (Fig. 1A). The IC_{50} of NHA was at least 100 μM greater than for all other cell lines, indicating that TBZ might be selective for tumor cells at certain concentrations (Fig. 1B). In the functional experiments, we then chose P3, representing a primary GBM cell line and U251, representing one of most common GBM laboratory cell lines. In the colony-forming assay, colony numbers were decreased by ~50% for P3 and U251 cells with 150 μM of TBZ and decreased by 90% for P3 and 75% for U251 with 300 μM of TBZ (Supplemental Fig. 1, A and B). Finally, the viability of P3 and U251 cells under treatment with different TBZ concentrations was less at 96 hours compared with 48 hours (Fig. 1C). These results indicated that TBZ potently reduced viability of GBM cells in a dose- and time-dependent manner.

Cell proliferation and cell cycle parameters were also examined in P3 and U251 cells under TBZ treatment. In P3 cells, EdU incorporation was reduced by 70% with 150 μM of TBZ and 90% with 300 μM of TBZ. In U251 cell lines, EdU incorporation was reduced by 40% with 150 μM of TBZ and by ~70% with 300 μM of TBZ. The EdU reduction in both P3 and U251 cell lines occurred in a dose-dependent manner with increasing TBZ concentrations (0, 150, and 300 μM) at 48 hours (Fig. 1D and Supplemental Fig. 1C). Cell cycle analysis further demonstrated that the percentage of GBM cells accumulated in G2/M increased under TBZ treatment in a dose-dependent manner (Fig. 1E and Supplemental Fig. 1D). Finally, in western blot analysis, proteins associated with cell proliferation and the G2/M checkpoint, including cyclin B1, cyclin B2, CDK1, and PCNA, were reduced in cells treated with TBZ.

Protein levels were all reduced by more than 60% in 300 μM of TBZ (Fig. 1F). These results demonstrated that levels of key checkpoint proteins paralleled cell cycle arrest induced by TBZ in GBM cell lines.

TBZ Inhibits Invasion of GBM Cells. To determine whether TBZ might inhibit infiltration capabilities of GBM cells, we examined GBM cells under TBZ treatment in transwell and Matrigel assays. In transwell assays, the number of P3 cells penetrating the membrane was reduced from >250 (0 μM of TBZ) to ~130 (150 μM of TBZ) and to no more than 60 (300 μM of TBZ). The number of invasive U251 cells was reduced from ~250 (0 μM of TBZ) to ~100 (150 μM of TBZ) and ~35 (300 μM of TBZ). After 48 hours of TBZ treatment, the number of cells in both cell lines was reduced in a dose-dependent manner relative to controls (0 μM; Fig. 2A). We also measured the invasive ability of GBM spheroids derived from P3 and U251 cells in suspension culture. The invasive areas of P3 spheres in Matrigel were also decreased to 65% (150 μM of TBZ) and 27% (300 μM of TBZ), and the invasive areas of U251 were decreased to 35% (150 μM of TBZ) and 17% (300 μM of TBZ) after exposure to TBZ relative to controls (0 μM of TBZ; Fig. 2B). Increasing TBZ concentrations further led to reduced invasion (Fig. 2B). In western blots performed on lysates prepared from P3 and U251 cells treated with TBZ, invasion-related proteins associated with EMT, such as N-cadherin, ZEB1, and MMP2, were downregulated >30% with 150 μM of TBZ and >50% with 300 μM of TBZ. Protein levels decreased in response to TBZ in a dose-dependent manner (Fig. 2C). These results indicated that TBZ suppressed invasion of GBM cells and inhibited expression of proteins involved in EMT.

MCM2 is Significantly Downregulated in TBZ-treated Glioma Cells. To identify potential gene targets of TBZ, we performed RNA sequencing on RNA isolated from GBM cells treated with the molecule. Gene ontology and Kyoto Encyclopedia of Genes and Genomes analysis of the resultant differentially expressed genes showed that TBZ treatment altered expression of genes associated with the cell cycle, mitosis, and DNA replication (Fig. 3, A and B). Through protein–protein interaction enrichment analysis, we selected out a protein–protein interaction network involving genes regulating the G2/M phase of the cell cycle (Fig. 3, C and D). Of the top ten differentially expressed genes in both P3 and U251 cell lines, *MCM2*, *ubiquitin with PHD and ring finger domains 1*, and *mini-chromosome maintenance complex component 5* showed the greatest difference in expression levels between treated and untreated cells (Fig. 3E). However, we found only MCM2 to be significantly downregulated at the protein level in both TBZ-treated P3 and U251 cell lines (Supplemental Fig. 2). Moreover, MCM2 protein levels decreased in a dose-dependent manner (Fig. 3F).

In Kaplan-Meier analysis performed with expression data from the TCGA and CGGA datasets, we found *MCM2* to be

(0, 100, 200, and 300 μM) and at different time points (24, 48, 72, and 96 hours). Data points are the OD450 values. All data are expressed as the mean ± S.D. of values from triplicate experiments. (D) Analysis of EdU-positive cells of P3 and U251 treated with different concentrations of TBZ for 48 hours. The percentage of EdU-positive cells (EdU-positive/DAPI-positive × 100%) was quantified in three random fields per sample. (E) Data points represent the percentage of cells in G0/G1 and G2/M in P3 and U251 at 48 hours after TBZ treatment. (F) Western blot to detect levels of cyclin B1, cyclin B2, CDK1, PCNA, and β-actin in P3 and U251. All data are expressed as the mean ± S.D. of values from triplicate experiments. ns = none-significant, $*P < 0.05$, $**P < 0.01$, and $***P < 0.001$ compared with controls.
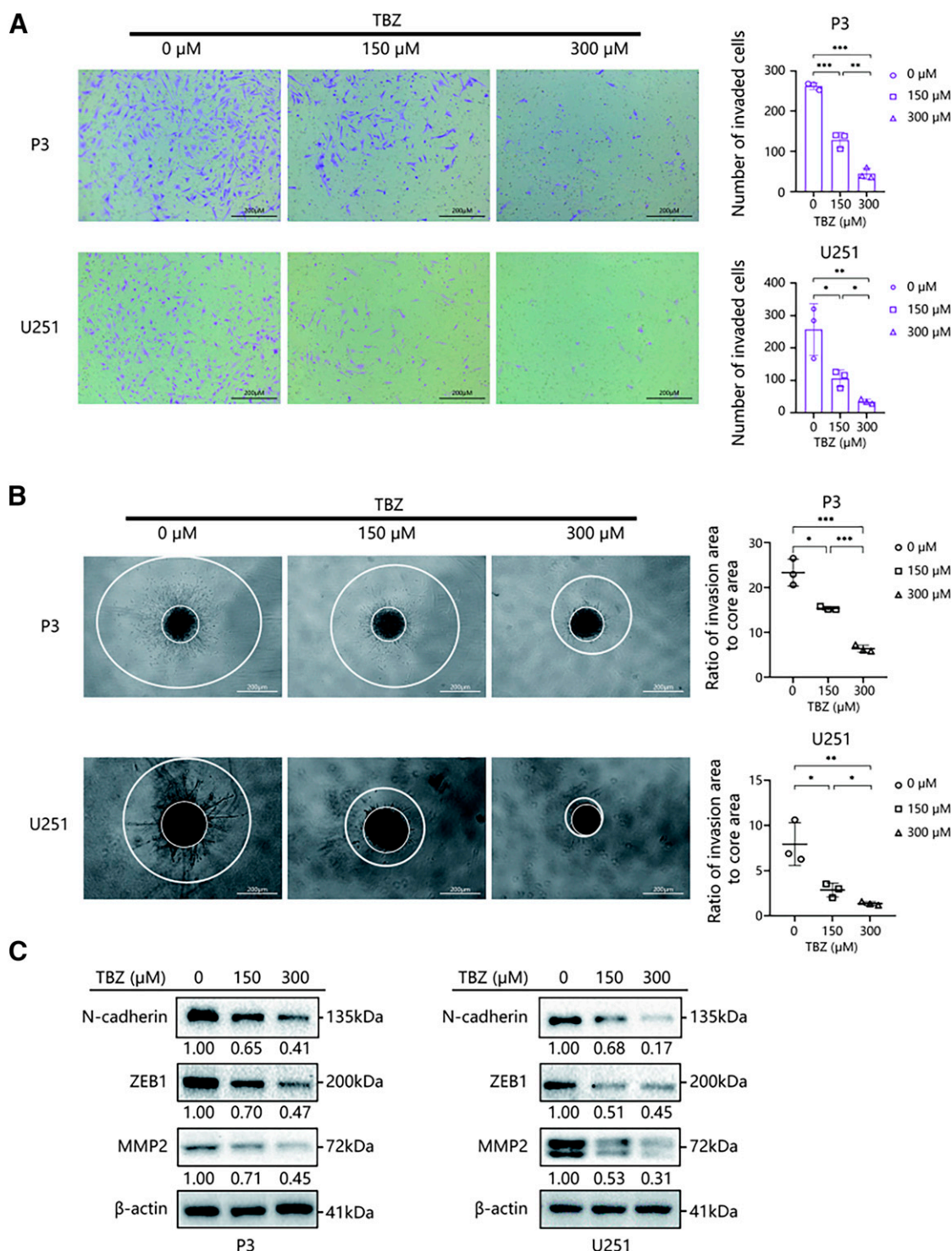
Fig. 2. Thiabendazole (TBZ) inhibits glioblastoma multiforme cell invasion. (A) Transwell invasion assays for P3 and U251 cell lines treated with TBZ (150 and 300 μM) or DMSO (0 μM). Graphic representation of transwell cell number for P3 and U251treated with TBZ (150 and 300 μM) or DMSO (0 μM). (B) 3D invasion assays for P3 and U251 (scale bars: 200 μm) treated with TBZ (150 and 300 μM) or DMSO (0 μM). Graphic representation of ratio values of the invasion area to the core area. (C) Western blot to determine expression levels of ZEB1, N-cadherin, MMP2, and β-actin (protein loading control) in P3 and U251 cells treated with DMSO or TBZ at the indicated concentrations for 48 hours. All data are expressed as the mean ± S.D. of values from triplicate experiments. *$P < 0.05$, **$P < 0.01$, and ***$P < 0.001$ compared with controls.

increased in GBM and low-grade gliomas. Furthermore, high expression of *MCM2* was related to poor survival of patients with glioma (Fig. 3, G and H). These results indicate that TBZ plays a role in causing G2/M cell cycle arrest in GBM cells, which may be mediated through the downregulation of MCM2. Thus, MCM might be a novel therapeutic target for the treatment of human glioma.

Knockdown of MCM2 Inhibits Glioma Cell Proliferation and Invasion. To determine whether loss of the putative TBZ target MCM2 suppressed GBM proliferation, we

A

R-HSA-69278: Cell Cycle, Mitotic
GO:0007059: chromosome segregation
R-HSA-69620: Cell Cycle Checkpoints
GO:0071103: DNA conformation change
GO:0007017: microtubule-based process
R-HSA-2299718: Condensation of Prophase Chromosomes
M129: PID PLK1 PATHWAY
M14: PID AURORA B PATHWAY
GO:1903046: meiotic cell cycle process
R-HSA-983231: Factors involved in megakaryocyte development and platelet production
GO:0000281: mitotic cytokinesis
GO:0010639: negative regulation of organelle organization
GO:0090068: positive regulation of cell cycle process
GO:0007062: sister chromatid cohesion
R-HSA-380320: Recruitment of NuMA to mitotic centrosomes
M46: PID ATR PATHWAY
CORUM:7542: KNL1-MIS12-NDC80-SPC24-ZWINT complex
CORUM:1108: DNA synthesome complex (15 subunits)
GO:0051640: organelle localization
GO:0000076: DNA replication checkpoint

B

Pathway Enrichment of Genes

C

Color	MCODE	Go	Description	Log10(P)
■	MCODE1	R-HSA-141424	Amplification of signal from the kinetochores	-35.4
■	MCODE1	R-HSA-141444	Amplification of signal from unattached kinetochores via a MAD2 inhibitory signal	-35.4
■	MCODE1	R-HSA-69618	Mitotic Spindle Checkpoint	-34.3
■	MCODE2	R-HSA-69278	Cell Cycle, Mitotic	-23.5
■	MCODE2	R-HSA-1640170	Cell Cycle	-22.3
■	MCODE2	R-HSA-69481	G2/M Checkpoints	-15.5
■	MCODE3	GO:0006260	DNA replication	-15.7
■	MCODE3	GO:0006261	DNA-dependent DNA replication	-14.6
■	MCODE3	R-HSA-176187	Activation of ATR in response to replication stress	-12.5

D

E

P3-Down

589 | 158 | 217

U251-Down

mRNA expression log2 fold change top10
(mRNA expersion >1000)

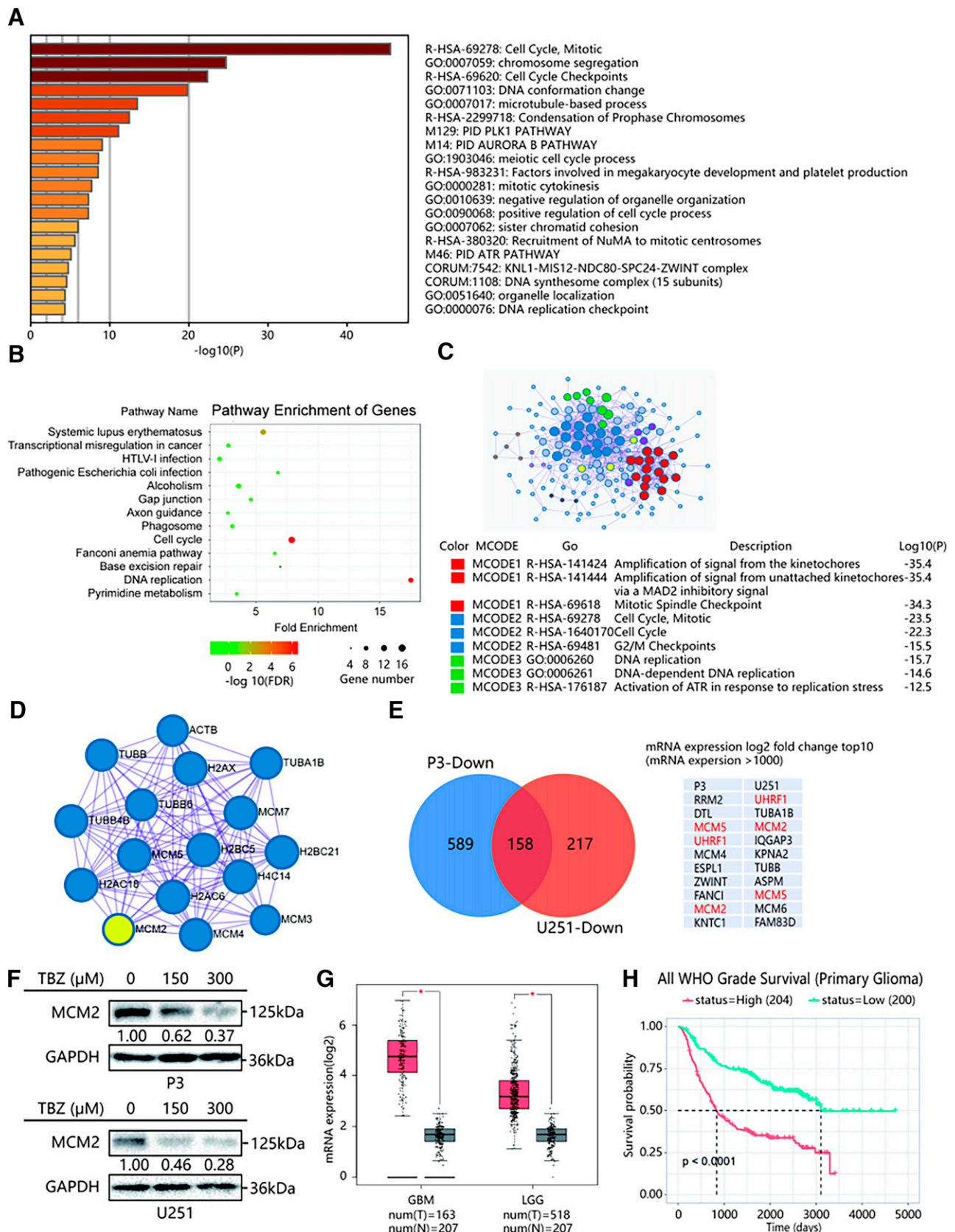| P3	U251
RRM2	UHRF1
DTL	TUBA1B
MCM5	MCM2
UHRF1	IQGAP3
MCM4	KPNA2
ESPL1	TUBB
ZWINT	ASPM
FANCI	MCM5
MCM2	MCM6
KNTC1	FAM83D

F

G

H

Fig. 3. Mini-chromosome maintenance complex component 2 (MCM2) mRNA and protein are downregulated by thiabendazole (TBZ) in glioblastoma multiforme cells in vitro. (A) Gene ontology analysis on the differentially expressed mRNAs identified by RNA sequencing of RNA isolated from TBZ-treated P3 and U251 cell lines versus controls. (B) Pathway enrichment analysis of the differentially expressed mRNAs identified through RNA sequencing of RNA isolated from TBZ-treated P3 and U251 cell lines compared with controls. (C) Protein–protein interaction enrichment analysis to predict genes interacting with other genes. (D) The network of protein–protein interaction derived from the differentially

used siRNA to knockdown MCM2 in P3 and U251 cells. In transfection experiments performed with three small-interfering MCM2 RNAs (si-RNA 799, si-RNA 1211, and si-RNA 1355), we found two siRNAs, si-RNA 799 and si-RNA 1355, to significantly reduce MCM2 protein levels in both cell lines (Fig. 4A). Cell viability was significantly reduced in si-RNA 1355-transfected P3 and si-RNA 799-transfected U251 after 48 hours (Fig. 4B). Examination of the cell cycle showed that MCM2 siRNA transfection led to an increase of cells in G2/M (11% of P3 and 14% of U251; Fig. 4, C and D). Loss of MCM2 also reduced invasion (44% for P3; 65% for U251) and migration (75% for P3; 60% for U251) of P3 and U251 cells as assessed in 3D invasion and transwell assays (Fig. 4, E and F and Supplemental Fig. 3). This reduced invasion, and migration was associated with decreased expression of invasion-related proteins N-cadherin (45% for P3; 37% for U251), ZEB1 (20% for P3; 37% for U251), and MMP2 (18% for P3; 28% for U251) in si-RNA-transfected P3 and U251 cells (Fig. 4G). Collectively, these data suggest that knockdown of MCM2 inhibits proliferation and invasion of GBM cells in vitro.

Overexpression of MCM2 Reverses TBZ-induced Suppression of GBM Cell Proliferation and Invasion. To determine whether increased MCM2 expression interfered with TBZ-induced growth arrest in GBM cells, we created stably expressing cells through infection with lentiviral constructs expressing MCM2. P3- and U251-MCM2-OE cells showed enhanced proliferation relative to uninfected or TBZ-treated cells (Fig. 5A). Overexpression of MCM2 led to a reduced percentage of cells (negative control; MCM2 overexpression, MCM2 OE; TBZ 300 μM; TBZ 300 μM + MCM2 OE) in G2/M under TBZ treatment (1.5% for U251 and 2.2% for P3, negative control versus MCM2 OE; 3% for U251 and 34% for P3, TBZ 300 μM versus TBZ 300 μM + MCM2 OE) (Fig. 5B and Supplemental Fig. 4). Moreover, proteins associated with cell proliferation and the G2/M checkpoint, including PCNA (10% for U251 and 45% for P3, negative control versus MCM2 OE; 78% for U251 and 208% for P3, TBZ 300 μM versus TBZ 300 μM + MCM2 OE), cyclin B1 (50% for U251 and 26% for P3, negative control versus MCM2 OE; 52% for U251, and 71% for P3, TBZ 300 μM versus TBZ 300 μM + MCM2 OE), cyclin B2 (27% for U251 and 31% for P3, negative control versus MCM2 OE; 63% for U251 and 73% for P3, TBZ 300 μM versus TBZ 300 μM + MCM2 OE), and CDK1 (147% for U251 and 62% for P3, negative control versus MCM2 OE; 133% for U251 and 212% for P3, TBZ 300 μM versus TBZ 300 μM + MCM2 OE), were increased in U251- and P3-MCM2-OE cells (Fig. 5C). Thus, overexpression of MCM2 rescued U251 and P3 cells from the TBZ-induced G2/M arrest. Finally, in 3D invasion and transwell assays, U251- and P3-MCM2-OE cells showed enhanced invasion (34% for U251 and 30% for P3, negative control versus MCM2 OE; 171% for U251, 88% for P3, TBZ 300 μM versus TBZ 300 μM + MCM2 OE) and

migration (29% for U251 and 23% for P3, negative control versus MCM2 OE; 206% for U251 and 163% for P3, TBZ 300 μM versus TBZ 300 μM + MCM2 OE) in the presence of TBZ (Fig. 5D and Supplemental Fig. 5). Invasion-related proteins, N-cadherin (89% for U251 and 66% for P3, negative control versus MCM2 OE; 174% for U251 and 129% for P3, TBZ 300 μM versus TBZ 300 μM + MCM2 OE), ZEB1 (68% for U251 and 49% for P3, negative control versus MCM2 OE; 21% for U251 and110% for P3, TBZ 300 μM versus TBZ 300 μM + MCM2 OE), and MMP2 (26% for U251 and 26% for P3, negative control versus MCM2 OE; 21% for U251 and 15% for P3, TBZ 300 μM versus TBZ 300 μM + MCM2 OE), were furthermore upregulated in U251- and P3-MCM2-OE cells (Fig. 5E). In conclusion, these results indicated that overexpression of MCM2 reversed TBZ-induced inhibition of proliferation and invasion in GBM cells.

TBZ Inhibits Growth of GBM Cells In Vivo. To examine whether TBZ inhibits GBM cell growth in vivo, we assessed its effects in a GBM tumor model derived from P3-luciferase-expressing cells intracranially implanted in nude mice. Tumor growth was monitored using luciferase bioluminescence. TBZ treatment significantly inhibited tumor growth compared with vehicle control in the mice (Figs. 6, A and B), and the weight of TBZ-treated mice also did not decrease as rapidly relative to controls at the 2- and 3-week time points after treatment (Fig. 6C). The day of death of control mice (DMSO) were as follows: day 32, 35, 39, 39, and 41. The day of death of the TBZ-treated mice were the following: day 39, 43, 44, 48, and 55. Kaplan-Meier analysis of the survival data also demonstrated a statistically significant difference for overall survival between control and TBZ-treated animals (median survival time 39 days versus 44 days, controls versus treated animals; Fig. 6D). Immunohistochemistry performed on tissue sections from xenografts demonstrated that Ki67, a marker of cell proliferation, was decreased by ∼50% in TBZ-treated tumors compared with untreated controls (Fig. 6E). In addition, the expression of MCM2 was significantly decreased in xenografts from TBZ-treated mice relative to controls. Thus, TBZ inhibited tumor cell growth in vivo, possibly through the suppression of MCM2 expression. We also examined the TBZ distribution in the brain tissue of nude mice by the liquid chromatography–tandem mass spectrometry assay. We found that the TBZ-treated sample had a transition of m/z 174.53–175.53 for an ion peak at 2.69 minutes (Supplemental Fig. 6). This value was consistent with that of the TBZ standard solution, confirming that TBZ is capable of delivery into the tumor area in the brain.

Discussion

Benzimidazole carbamate derivatives are approved compounds for the treatment of parasitic diseases in humans.

---

expressed genes associated with the cell cycle. (E) Top ten genes with greatest fold change in mRNA expression levels (fold change value >1000) in P3 and U251, respectively. Intersecting genes, *MCM2, mini-chromosome maintenance complex component 5, ubiquitin with PHD and ring finger domains 1,* downregulated in P3 and U251 cells are highlighted in red. (F) Western blot to determine expression levels of MCM2 and GAPDH (protein loading control) in P3 and U251 cells treated with DMSO or TBZ at the indicated concentrations for 48 hours. (G) Analysis of expression levels of *MCM2* mRNA in normal brain tissue samples and glioblastoma multiforme samples in the publicly available database TCGA. *P < 0.05. (H) Kaplan-Meier analyses to determine differences in overall survival for patients with low and high *MCM2* expressing primary gliomas. High MCM2 expression group expresses more MCM2 than median expression, while low MCM2 expression group expresses less MCM2 than median expression. The data were obtained from the CGGA database.
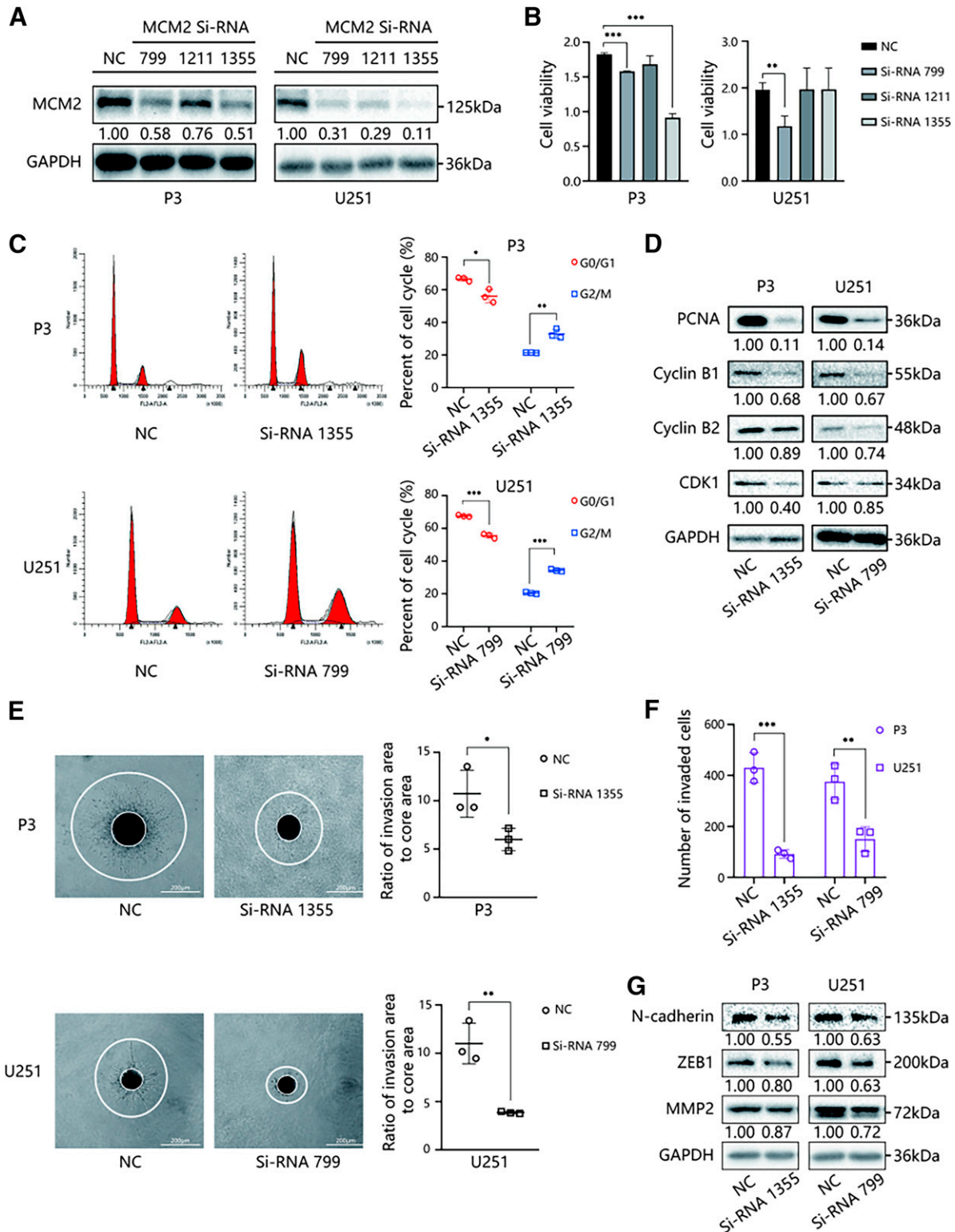
Fig. 4. Knockdown of mini-chromosome maintenance complex component (MCM2) inhibits glioblastoma multiforme cell proliferation and invasion. (A) Western blot to assess knockdown efficiency of MCM2 by siRNA in P3 and U251 cells. (B) Cell Counting Kit-8 assays to measure cell viability of P3 and U251 transfected with MCM2 and control si-RNAs. Data points are OD450 values. **$P < 0.01$, ***$P < 0.001$. (C) Cell cycle distribution of P3 and U251 determined with propridium iodide staining by flow cytometry analysis. Data points are the percentage of cells in G0/G1 and G2/M in P3 and U251 at 48 hours after si-RNA transfection. *$P < 0.05$, **$P < 0.01$, and ***$P < 0.001$. (D) Western blot to detect expression levels of PCNA, cyclin B1, cyclin B2, CDK1, and GAPDH (protein loading control) in P3 and U251 cells 48 hours after si-RNA transfection. (E) 3D invasion assays for P3 and U251 transfected with MCM2 or control si-RNA (scale bars: 200 μm). Graphic representation of the ratio values of the invasion area to the core area. *$P < 0.05$, **$P < 0.01$. (F) Quantification of transwell cell number for P3 and U251cells transfected with MCM2 or control si-RNA. ** $P < 0.01$, ***$P < 0.001$. (G) Western blot to determine expression levels of N-cadherin, ZEB1, MMP2, and GAPDH in P3 and U251 transfected with MCM2 or control siRNA.
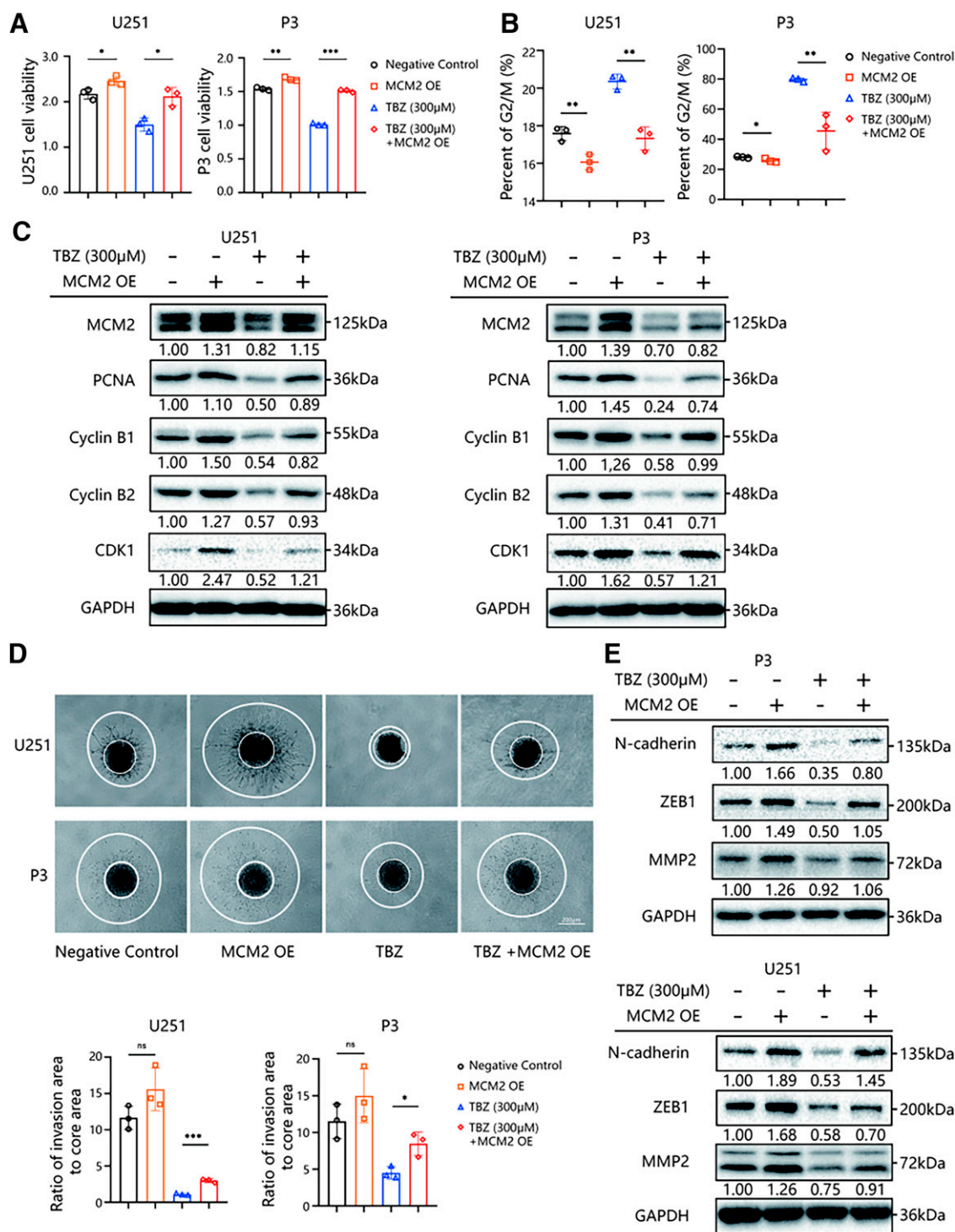
Fig. 5. Overexpression of mini-chromosome maintenance complex component (MCM2) rescues glioblastoma multiforme cells from thiabendazole inhibition. (A) Cell Counting Kit-8 assays to measure cell viability of P3- and U251-MCM2-OE and parental cell lines under the conditions indicated. (B) The percentage of cells in G2/M in the four treatment groups. (C) Western blot to determine expression levels of MCM2, PCNA, cyclin B1, cyclin B2, CDK1, and GAPDH in P3- and U251-MCM2-OE and parental cell lines under the conditions indicated. (D) 3D invasion assays for P3- and U251-MCM2-OE and parental cell lines under the conditions indicated (scale bars: 200 μm). Graphic representation of ratio values of the invasion area to the core area. (E) Western blot to detect expression levels of N-cadherin, ZEB1, MMP2, and GAPDH in P3- and U251-MCM2-OE and parental cell lines under the conditions indicated. All data are expressed as the mean ± S.D. of values from triplicate experiments. ns = none-significant, $*P < 0.05$, $**P < 0.01$, and $***P < 0.001$.

Such compounds include mebendazole, albendazole, fenbendazole, thiabendazole, and flubendazole. They kill worms by binding and inhibiting beta-tubulin (Cumino et al., 2009). TBZ was approved by the United States Food and Drug Administration in 1967 for use in humans and has been used as antifungal treatment for half a century. Previous reports indicated
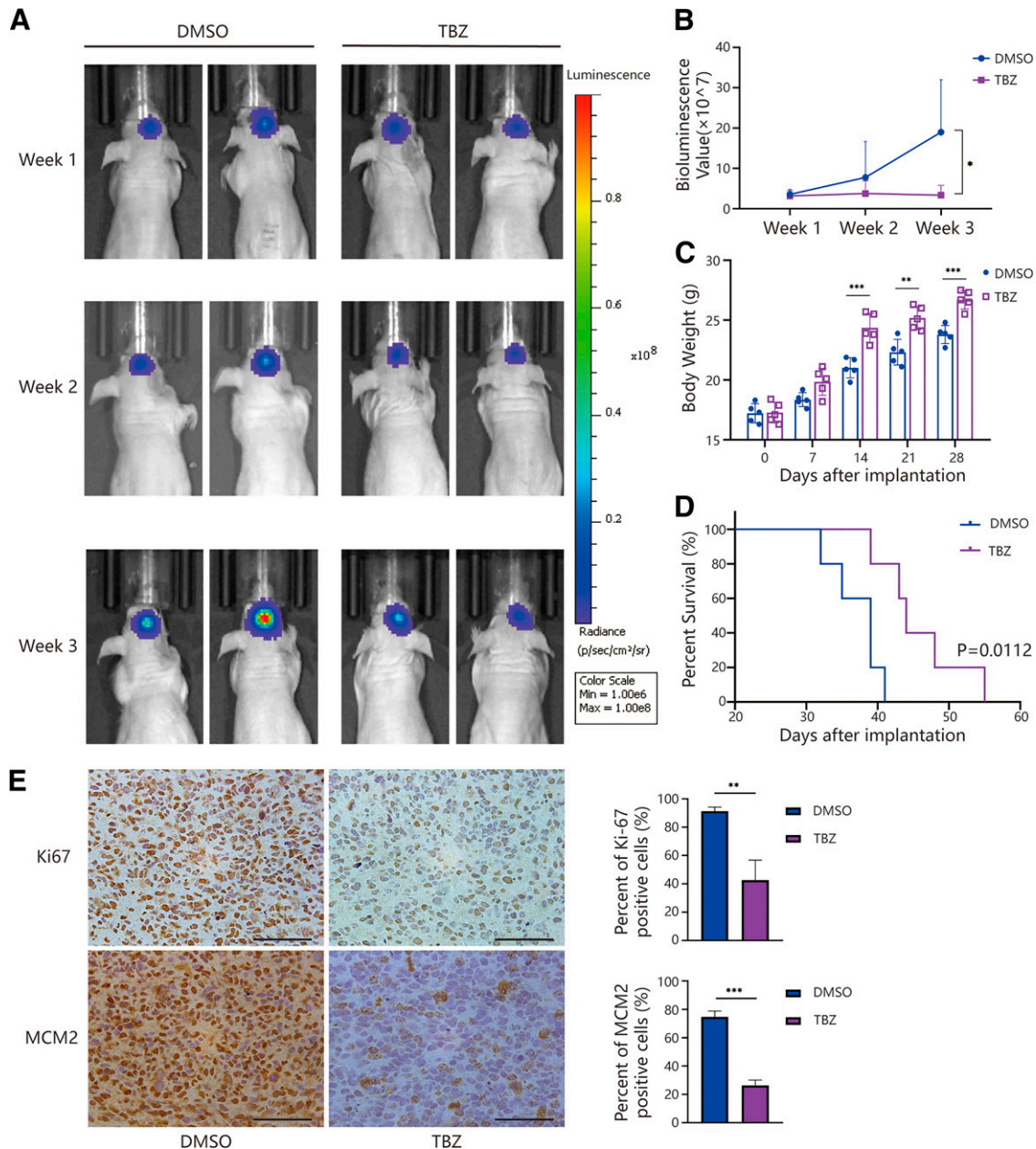
Fig. 6. Thiabendazole inhibits tumor growth in an orthotopic model for glioblastoma multiforme in mice. (A) P3-luciferase cells were orthotopically implanted into nude mice, and tumor growth was followed by the detection of bioluminescent signals under the PerkinElmer IVIS Spectrum at days 7, 14, and 21 after implantation. (B) Quantification of bioluminescence values to determine tumor growth at days 7, 14, and 21. (C) Quantification of the weight of nude mice in each experimental group at days 0, 7, 14, 21, and 28. (D) Kaplan-Meier analysis to determine overall survival of tumor bearing nude mice and log-rank test to assess the statistical significance of the differences. (E) Immunohistochemistry staining for Ki67 and MCM2 in the tumor sections of nude mice from each group as indicated (scale bars: 100 μm). Graphic representation of the percentage of Ki-67 and MCM2 positive cells in the tumor sections. All data are expressed as the mean ± S.D. of values from triplicate samples. *$P < 0.05$, **$P < 0.01$, ***$P < 0.001$ compared between the two treatments.

that TBZ has antitumor effects in melanoma and fibrosarcoma, including inhibition of proliferation and migration in melanoma B16F10 cells and angiogenesis in fibrosarcoma (Zhang et al., 2013). These potential antineoplastic properties render TBZ to be of possible value as a repurposed drug for the treatment of GBM. In this study, we demonstrated that TBZ inhibited cell viability of several GBM cell lines, including P3, U251, LN229, and U118MG. The molecule suppressed proliferation of GBM cells (P3 and U251) by inducing G2/M arrest. Moreover, TBZ reduced invasion and migration of GBM cells.

Loss of cell cycle checkpoint control underlies the aggressive proliferation and dysregulation of the cell cycle associated with GBM. Thus, therapies have been designed to inhibit the cell cycle (Dominguez-Brauer et al., 2015). The mechanism of action of many microtubule inhibitors involves inhibition of the G2/M phase (Castro-Gamero et al., 2018). These drugs may be synergistic with the current standard of GBM therapy (temozolomide or radiotherapy), either by facilitating DNA damage or sensitizing malignant cells to standard therapy (Vitovcova et al., 2020). In future studies, we plan to explore

the effect of the combination treatment of TBZ, TMZ, and radiotherapy on GBM.

RNA sequencing revealed potential targets of TBZ in GBM cells. Using gene ontology, Kyoto Encyclopedia of Genes and Genomes, and protein–protein interaction network analysis, we found that TBZ regulates the expression of proteins that function in cell proliferation and the cell cycle. MCM2 was among the most highly differentially expressed genes under TBZ treatment, and overexpression of the gene rescued TBZ-treated cells from inhibition of cell growth. As the cytotoxic effect of TBZ ($>IC_{50}$) was lower in NHA than in GBM cells, the molecule might be selective for tumor cells at certain concentrations in the clinical management of patients.

The function of MCM is regulated at elongation and termination of DNA replication (Brewster and Chen, 2010; Li et al., 2015; Seo and Kang, 2018). In the process of carcinogenesis, the dysfunction of MCM generates instability in the structure of the DNA fork, thus creating conditions for the acquisition of the gene mutations driving tumor development. As a member of the MCM family, MCM2 has been shown to be overexpressed in various tumors, including hepatocellular carcinoma (Yang et al., 2018; Yang et al., 2019), pancreatic adenocarcinoma (Peng et al., 2016; Xi and Zhang, 2018), lung cancer (Cheung et al., 2017), breast carcinoma (Yousef et al., 2017; Issac et al., 2019), ovarian cancer (Deng et al., 2019), and cervical cancer (Mukherjee et al., 2007; Amaro Filho et al., 2014). MCM2 was predicted to be a valuable prognostic biomarker in breast cancer (Liu et al., 2021), cervical cancer (Wu and Xi, 2021), and neuroendocrine prostate cancer (Hsu et al., 2021). In addition, MCM2 was suggested to be a potential treatment target to breast cancer and prostate cancer (Hsu et al., 2021; Liu et al., 2021). In neuroblastoma, MCM2 expression is positively correlated with tumor growth, and thus the gene is a novel potential target for neuroblastoma pharmacological treatment (Garbati et al., 2020). Our bioinformatic analysis showed that *MCM2* is upregulated in GBM tissue (TCGA) and related to decreased survival in patients with glioma (CGGA). Silencing MCM2 through siRNA knockdown inhibited proliferation and invasion of GBM cells. In contrast, the overexpression of MCM2 partially rescued GBM cells from cell cycle arrest and reduced invasion under TBZ treatment. These results suggest that MCM2 is a critical molecular target of TBZ and warrants further study as a biomarker for TBZ as a potential treatment of GBM.

In summary, TBZ inhibits the proliferation of GBM by inducing a G2/M phase cell cycle arrest and suppresses the invasion of GBM tumor cells. TBZ downregulated the expression of MCM2, which is overexpressed in GBM based on analysis of publicly available datasets. Knockdown of MCM2 decreased GBM tumor growth and invasion in vitro, and TBZ inhibits growth of GBM cells in vivo. These findings thus warrant further investigation into repurposing TBZ for the treatment of patients with GBM. However, although TBZ does slow tumor growth in our animal model, eventually the tumor kills tumor-bearing mice, possibly due to TBZ-resistant tumor cells. This recovery phase under TBZ treatment would therefore also be of interest to study in the future.

Authorship Contributions

Participated in research design: Yaotian Hu, Wenjing Zhou, Jian Wang.

Conducted experiments: Yaotian Hu, Zhiyi Xue, Xuemeng Liu, Xun Zhang, Zichao Feng, Wenjie Li and Qing Zhang.

Performed data analysis: Yaotian Hu and Xiaofei Liu.

Wrote or contributed to the writing of the manuscript: Yaotian Hu, Yulin Zhang, Xiaofei Liu, Wenjie Li, Qing Zhang, Anjing Chen, Bin Huang, and Jian Wang.

References

Amaro Filho SM, Nuovo GJ, Cunha CB, Ramos Pereira LdeO, Oliveira-Silva M, Russomano F, Pires A, and Nicol AF (2014) Correlation of MCM2 detection with stage and virology of cervical cancer. *Int J Biol Markers* 29:e363–e371.

Bai RY, Staedtke V, Aprhys CM, Gallia GL, and Riggins GJ (2011) Antiparasitic mebendazole shows survival benefit in 2 preclinical models of glioblastoma multiforme. *Neuro-oncol* 13:974–982.

Bell Jr E and Karnosh LJ (1949) Cerebral hemispherectomy; report of a case 10 years after operation. *J Neurosurg* 6:285–293.

Brennan CW, Verhaak RG, McKenna A, Campos B, Noushmehr H, Salama SR, Zheng S, Chakravarty D, Sanborn JZ, Berman SH et al.; TCGA Research Network (2013) The somatic genomic landscape of glioblastoma. *Cell* 155:462–477.

Brewster AS and Chen XS (2010) Insights into the MCM functional mechanism: lessons learned from the archaeal MCM complex. *Crit Rev Biochem Mol Biol* 45:243–256.

Campbell WC and Cuckler AC (1969) Thiabendazole in the treatment and control of parasitic infections in man. *Tex Rep Biol Med* 27 (Suppl 2):2, 665.

Castro-Gamero AM, Pezuk JA, Brassesco MS, and Tone LG (2018) G2/M inhibitors as pharmacotherapeutic opportunities for glioblastoma: the old, the new, and the future. *Cancer Biol Med* 15:354–374.

Cha HJ, Byrom M, Mead PE, Ellington AD, Wallingford JB, and Marcotte EM (2012) Evolutionarily repurposed networks reveal the well-known antifungal drug thiabendazole to be a novel vascular disrupting agent. *PLoS Biol* 10:e1001379.

Cheung CHY, Hsu CL, Chen KP, Chong ST, Wu CH, Huang HC, and Juan HF (2017) MCM2-regulated functional networks in lung cancer by multi-dimensional proteomic approach. *Sci Rep* 7:13302.

Cumino AC, Elissondo MC, and Denegri GM (2009) Flubendazole interferes with a wide spectrum of cell homeostatic mechanisms in Echinococcus granulosus protoscoleces. *Parasitol Int* 58:270–277.

Darlix A, Zouaoui S, Rigau V, Bessaoud F, Figarella-Branger D, Mathieu-Daudé H, Trétarre B, Bauchet F, Duffau H, Taillandier L et al. (2017) Erratum to: Epidemiology for primary brain tumors: a nationwide population-based study. *J Neurooncol* 131:547.

Deng M, Sun J, Xie S, Zhen H, Wang Y, Zhong A, Zhang H, Lu R, and Guo L (2019) Inhibition of MCM2 enhances the sensitivity of ovarian cancer cell to carboplatin. *Mol Med Rep* 20:2258–2266.

Dominguez-Brauer C, Thu KL, Mason JM, Blaser H, Bray MR, and Mak TW (2015) Targeting mitosis in cancer: emerging strategies. *Mol Cell* 60:524–536.

Gallia GL, Holdhoff M, Brem H, Joshi AD, Hann CL, Bai RY, Staedtke V, Blakeley JO, Sengupta S, Jarrell TC et al. (2021) Mebendazole and temozolomide in patients with newly diagnosed high-grade gliomas: results of a phase 1 clinical trial. *Neuro-oncol Adv* 3:vdaa154.

Garbati P, Barbieri R, Cangelosi D, Zanon C, Costa D, Eva A, Thellung S, Calderoni M, Baldini F, Tonini GP et al. (2020) MCM2 and carbonic anhydrase 9 are novel potential targets for neuroblastoma pharmacological treatment. *Biomedicines* 8:471.

Gosselin RE, Smith RP, and Hodge HC (1984) *ClinicalTtoxicology of Commercial Products*, Williams & Wilkins, Baltimore.

Hsu EC, Shen M, Aslan M, Liu S, Kumar M, Garcia-Marques F, Nguyen HM, Nolley R, Pitteri SJ, Corey E et al. (2021) MCM2-7 complex is a novel druggable target for neuroendocrine prostate cancer. *Sci Rep* 11:13305.

Issac MSM, Yousef E, Tahir MR, and Gaboury LA (2019) MCM2, MCM4, and MCM6 in breast cancer: clinical utility in diagnosis and prognosis. *Neoplasia* 21:1015–1035.

Kong Y, Feng Z, Chen A, Qi Q, Han M, Wang S, Zhang Y, Zhang X, Yang N, Wang J et al. (2019) The natural flavonoid galangin elicits apoptosis, pyroptosis, and autophagy in glioblastoma. *Front Oncol* 9:942.

Lee SY (2016) Temozolomide resistance in glioblastoma multiforme. *Genes Dis* 3:198–210.

Li N, Zhai Y, Zhang Y, Li W, Yang M, Lei J, Tye BK, and Gao N (2015) Structure of the eukaryotic MCM complex at 3.8 Å. *Nature* 524:186–191.

Liu X, Liu Y, Wang Q, Song S, Feng L, and Shi C (2021) The alterations and potential roles of MCMs in breast cancer. *J Oncol* 2021:7928937.

Mukherjee G, Muralidhar B, Bafna UD, Laskey RA, and Coleman N (2007) MCM immunocytochemistry as a first line cervical screening test in developing countries: a prospective cohort study in a regional cancer centre in India. *Br J Cancer* 96:1107–1111.

Ostrom QT, Patil N, Cioffi G, Waite K, Kruchko C, and Barnholtz-Sloan JS (2020) CBTRUS Statistical report: primary brain and other central nervous system tumors diagnosed in the United States in 2013-2017. *Neuro-oncol* 22(12, Suppl 2)iv1–iv96.

Peng YP, Zhu Y, Yin LD, Zhang JJ, Guo S, Fu Y, Miao Y, and Wei JS (2016) The expression and prognostic roles of MCMs in pancreatic cancer. *PLoS One* 11:e0164150.

Seo YS and Kang YH (2018) The human replicative helicase, the CMG complex, as a target for anti-cancer therapy. *Front Mol Biosci* **5**:26.

Shergalis A, Bankhead 3rd A, Luesakul U, Muangsin N, and Neamati N (2018) Current challenges and opportunities in treating glioblastoma. *Pharmacol Rev* **70**:412–445.

Stupp R, Mason WP, van den Bent MJ, Weller M, Fisher B, Taphoorn MJ, Belanger K, Brandes AA, Marosi C, Bogdahn U et al.; European Organisation for Research and Treatment of Cancer Brain Tumor and Radiotherapy Groups; National Cancer Institute of Canada Clinical Trials Group (2005) Radiotherapy plus concomitant and adjuvant temozolomide for glioblastoma. *N Engl J Med* **352**:987–996.

Vitovcova B, Skarkova V, Rudolf K, and Rudolf E (2020) Biology of glioblastoma multiforme-exploration of mitotic catastrophe as a potential treatment modality. *Int J Mol Sci* **21**:15.

Whalen GE, Rosenberg EB, Gutman RA, Cross J, Fresh JW, Strickland T, and Uylangco C (1971) Treatment of intestinal capillariasis with thiabendazole, bithionol, and bephenium. *Am J Trop Med Hyg* **20**:95–100.

Wu B and Xi S (2021) Bioinformatics analysis of the transcriptional expression of minichromosome maintenance proteins as potential indicators of survival in patients with cervical cancer. *BMC Cancer* **21**:928.

Xi T and Zhang G (2018) Integrated analysis of tumor differentiation genes in pancreatic adenocarcinoma. *PLoS One* **13**:e0193427.

Yang J, Xie Q, Zhou H, Chang L, Wei W, Wang Y, Li H, Deng Z, Xiao Y, Wu J et al. (2018) Proteomic analysis and NIR-II imaging of MCM2 protein in hepatocellular carcinoma. *J Proteome Res* **17**:2428–2439.

Yang WX, Pan YY, and You CG (2019) CDK1, CCNB1, CDC20, BUB1, MAD2L1, MCM3, BUB1B, MCM2, and RFC4 may be potential therapeutic targets for hepatocellular carcinoma using integrated bioinformatic analysis. *BioMed Res Int* **2019**:1245072.

Yousef EM, Furrer D, Laperriere DL, Tahir MR, Mader S, Diorio C, and Gaboury LA (2017) MCM2: an alternative to Ki-67 for measuring breast cancer cell proliferation. *Mod Pathol* **30**:682–697.

Zhang J, Zhao C, Gao Y, Jiang Y, Liang H, and Zhao G (2013) Thiabendazole, a well-known antifungal drug, exhibits anti-metastatic melanoma B16F10 activity via inhibiting VEGF expression and inducing apoptosis. *Pharmazie* **68**:962–968.

Address correspondence to: Jian Wang, Institute of Brain Inspired Science, 107 Wenhoa Xi Road, Jinan, 250012, China. E-mail: jian.wang@uib.no